Wavelet Analysis of Simulated Tropical Convective Cloud Systems. Part II: Decomposition of Convective-Scale and Mesoscale Structure

JUN-ICHI YANO

Cooperative Research Centre for Southern Hemisphere Meteorology, Monash University, Clayton, Victoria, Australia

MITCHELL W. MONCRIEFF AND XIAOQING WU

National Center for Atmospheric Research, Boulder, Colorado*

(Manuscript received 8 February 2000, in final form 21 July 2000)

ABSTRACT

Numerically simulated three-dimensional tropical convective systems were analyzed using a wavelet approach in which the vertical shear of the ambient wind is used as a decomposition criterion. The method objectively decomposes the simulated systems into their two primary components, namely organized deep convection and a mesoscale stratiform region. This reproduces the standard model of highly organized mesoscale convective systems as well as giving an objective characterization of less organized regimes. It demonstrates the vertical component of wind shear as a statistically useful criterion in addition to its better known role as a quasi-deterministic mechanism controlling the organization of convection and its scale selection.

1. Introduction

Precipitating convection is known to be organized into various kinds of cloud systems on scales ranging from a few kilometers to more than a thousand kilometers, which is the entire range of mesoscale motion. Their ubiquity and structural diversity are amply illustrated in visible and infrared satellite images. One prominent kind of organization is the mesoscale convective system, also known as a tropical cloud cluster, which is an ensemble of cumulonimbus consisting of two primary interactive scales of motion (Houze 1997). First, the convective region of scale about 10 km is identified with strong updrafts and downdrafts and intense precipitation. Second, the mesoscale region is characterized by weak vertical motion, widespread light precipitation, and cirrus anvils on a scale of hundreds of kilometers. The accompanying mesoscale descent is driven by evaporative cooling and, in part, by the convectively generated pressure gradient.[1]

The lifetime of a typical mesoscale convective system greatly exceeds that of the attendant cumulonimbus in the convective region. The best organized and most persistent are squall lines that maintain a quasi-steady structure for days and can travel thousands of kilometers. The archetypal dynamics of squall lines were described by Moncrieff (1992) as an analytic paradigm of the standard conceptual model derived from observational analysis (Houze et al. 1989). Another kind of organization, for which no closed theory exists, is in the form of nonsquall cloud clusters, which are ensembles of cumulonimbus. These two categories of organization are the primary focus herein.

In a formal sense a mesoscale system is similar to a coherent structure in turbulent flow but its physical origin is distinct from the coherent vortices associated with geophysical turbulence (e.g., McWilliams and Weiss 1994). Rather than being a product of nonlinear energy transfer in wavenumber space, manifested as

* The National Center for Atmospheric Research is sponsored by the National Science Foundation.

Corresponding author address: Jun-Ichi Yano, Meteorologisches Institut, Universität Hamburg, Bundesstraße 55, D-20146 Hamburg, Germany.
E-mail: yano@dkrz.de

[1] The convective and mesoscale components are defined by the two horizontal scales identified in Part I (Yano et al. 2001), in accordance with mesoscale etymology. Herein, ''stratiform'' is part of the ''mesoscale component'' and ''mesoscale convective system'' identifies the convective system defined by these two components. This is only a slightly different terminology from Houze (1997), who distinguishes ''convective'' and ''stratiform'' in terms of physics and morphology.

vortex–vortex interaction in physical space, the coherence associated with mesoscale systems stems from the organizing effect of wind shear on latent heating (condensation and freezing) and interactions among these quantities. Only a small fraction of water vapor condenses and only a fraction of condensed water precipitates, the remainder evaporates and generates potential energy for downdrafts. Downdrafts are important not only in mesoscale organization at large but they also initiate convection through dynamical lifting at the attendant (density current) outflow fronts. Only in highly organized squall lines are the relationships among density currents, downdrafts, and mesoscale organization reasonably understood. The reader is referred to Cotton and Anthes (1989) for a review of mesoscale convective systems.

In Part I of this two-part paper, we investigated the two-scale structure of organized convective cloud systems characterized by convective-scale and mesoscale components using a wavelet approach. In Part II, we decompose the system into these two scales using this method. Because wind shear fundamentally affects the organization of convection, we use this quantity as a criterion for our decomposition in wavelet space.

This paper is organized as follows. We review the synthetic dataset in section 2. The decomposition analyses are presented in section 3, and the paper concludes with section 4.

2. Convective cloud system simulations: The synthetic dataset

Observations alone seldom provide datasets with high enough resolution and dynamical consistency for definitive investigations of the statistical behavior of convection. A strength of cloud-resolving models is their provision of reasonably complete and consistent synthetic data. Particularly suitable for statistical analysis are realizations of tropical cloud systems in a state of convective-radiative quasi-equilibrium. These systems evolve, over a period of days, from random perturbations of a horizontally homogeneous initial state. Numerical models do not presently have domains big enough to allow the explicitly resolved convective scale to feed back to large scales. Therefore, the effect of the large-scale fields on convection is specified as *external time-varying forcing* that generates convective available potential energy through temperature and moisture advection, through surface fluxes of heat, moisture, and momentum and through cloud-interactive radiative flux divergence. This type of modeling enables realistic systems to be simulated even if simple parameterizations of cloud microphysical processes are employed (Wu et al. 1997; Moncrieff 1995).

We use a three-dimensional simulation of the mesoscale convective system during Phase III of GATE reported in Wu and Moncrieff (1996) and Grabowski et al. (1998, hereafter GWMH), in which the focus was on the domain-averaged budgets. In this two-part work we focus attention on the structure of the simulated convective systems. The horizontal domain used for the simulation is 400 km $\times$ 400 km with 2-km horizontal grid length. A 42-level stretched grid is used in the vertical direction. Horizontally, we interpolate the data into 128 $\times$ 128 grid points, because a power of two is required for the wavelet analysis. In the vertical direction we interpolate onto a homogeneous grid of points with 0.5-km grid length, and use the lowest 16 km for the analysis, as in GWMH. The other aspects are summarized in Part I and details are given in the references therein.

3. Wavelet analysis of the simulated cloud systems

We use synthetic data provided by the GWMH cloud-resolving three-dimensional simulation, noting that the periodic lateral boundary conditions are ideal for a wavelet analysis. Because the organizing effect of shear produces multiscale spatial localization, neither standard statistical analyses in physical space (which lose the scale-dependent characterization) nor decompositions in Fourier space (which lose the space localization) are adequate. Wavelet analysis provides a more optimal basis for objectively decomposing the localized multiscale structure because it preserves both aforementioned characteristics (cf. Farge 1992). In particular, we will show that the wavelets can depict the mesoscale stratiform region as a continuous field with embedded convective-scale components. This contrasts with the standard columnwise decomposition, in which the continuous stratiform precipitation is detached from an intermittent distribution of the convective regions.

a. Discrete wavelet analysis

As in Part I, the Meyer wavelet (Meyer 1992) is used. Meyer's discrete wavelets are basis functions that expand a periodic function in a finite domain ($0 \leq x \leq L$). Spatial localization and scale characterizations are represented as follows. The wavelets $\phi_{k,j}(x)$ are characterized by two integer parameters (we use a slightly different definition of the subscripts from Part I): the wavenumber k measures the spatial scale, and an index j measures the spatial localization (location) of the wavelet peak. The wavenumber k is a power of two, namely $k = 2^i$ where $i = 0, 1, 2, \ldots$ counted in descending direction from the top row in Fig. 4 of Part I. For a given integer wavenumber k, the wavelets represent the modes localized at k different spatial locations, which are constructed by shifting a wavelet form through an equal interval. This spatial shift is indicated by the index j, which increases from $j = 1$ to $j = k$ as the wavelet localization (identified by its maximum) shifts from left to right.

These wavelets are complete (in the same sense as

for a Fourier expansion) and satisfy the orthogonality condition

$$\frac{1}{L}\int_0^L \phi_{k,j}(x)\phi_{k',j'}(x)\,dx = \delta_{kk'}\delta_{jj'}, \tag{1}$$

where $\delta_{kk'}$, $\delta_{jj'}$ are Kronecker's deltas. By virtue of orthogonality, any periodic function $f(x)$ in the domain $0 \le x \le L$ can be expanded as

$$f(x) = \sum_{i=0}^{i_{\max}} \sum_{j=1}^{2^i} \hat{f}_{2^i,j}\phi_{2^i,j}(x) + \overline{f}, \tag{2}$$

where the wavelet coefficients are determined by

$$\hat{f}_{k,j} = \frac{1}{L}\int_0^L f(x)\phi_{k,j}(x)\,dx \tag{3}$$

and the maximum wavenumber $k_{\max} = 2^{i_{\max}}$ is equal to half of the total spatial grid points of the data. Equation (3) may be considered as the definition of the wavelet transform (in analogy to the Fourier transform). The last term in Eq. (2) is the domain average $\overline{f} \equiv (\int_0^L f(x)\,dx)/L$, which can be included as a part of the expansion by introducing a constant wavelet $\phi_{0,1}(x) = 1$ as in Part I.

We apply this wavelet transform sequentially to each horizontal section, (x, y), of the double-periodic simulated fields, that is,

$$f(x, y, z) = \sum_{l_x=1}^{N_x} \sum_{l_y=1}^{N_y} \hat{f}(l_x, l_y, z)\phi_{l_x}(x)\phi_{l_y}(y). \tag{4}$$

Here, l_x and l_y are indices for the two horizontal directions, defined by combining the two wavelet parameters as $l = k + j$ and $l = 1$ for $k = 0$; N_x and N_y are the number of the data points in the x and y directions, respectively. The wavelet coefficients $\hat{f}_{l_x l_y}(z)$ are defined as an analytic extension of the one-dimensional case in Eq. (3). Note that the wavelet transform is not applied in the vertical (z) direction because the boundary conditions at top and bottom are not periodic. The two-dimensional wavelet coefficients constitute the wavelet space, in analogy with the Fourier space.

As in Part I, we analyze snapshots of each of three distinctive cloud system regimes—a squall line, a nonsquall cloud cluster, and scattered convection—generated spontaneously in the cloud-resolving model as the large-scale forcing and shear evolve.

b. Decomposition method

The simulated systems are decomposed into the various dynamical components using the invertibility principal of the wavelet coefficients into real (physical) space (Fig. 1). The wavelet transformation [Eq. (3)] is applied to a set of variables consisting of wind vector $\mathbf{v}$, total water condensate t_c, water moisture density q, temperature θ, etc., which can be considered a vector $\mathbf{f}(x, y, z) = (f_1, f_2, f_3, \ldots, f_m)$, where m is the number

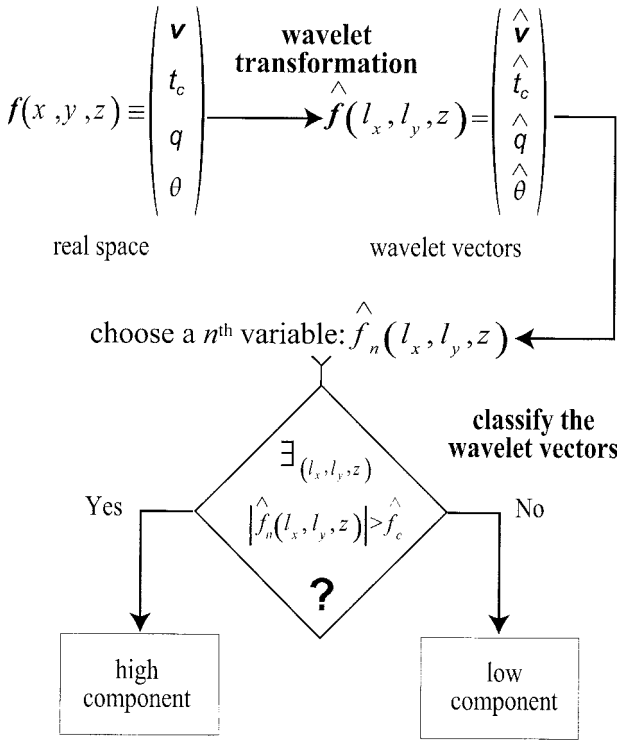

FIG. 1. Flow chart for the wavelet decomposition. See text for details.

of variables. We obtain the wavelet vector $\hat{\mathbf{f}}(l_x, l_y, z)$ of the corresponding wavelet coefficients.

It was shown in Part I that the two-scale structure of the mesoscale convective system is realistically depicted in wavelet space, implying that wavelet space, rather than physical space, is the appropriate decomposition medium. In order to implement this idea we define the following general principle. After applying the wavelet transformation, we choose a particular variable (say, $\hat{f}_n$) which can physically distinguish one dynamical component from another. We classify the wavelet vectors $\hat{\mathbf{f}}(l_x, l_y, z)$ into two sets, namely the high component, $\hat{\mathbf{f}}_H(l_x, l_y, z)$, and the low component, $\hat{\mathbf{f}}_L(l_x, l_y, z)$, depending on whether the absolute value for the wavelet coefficient of this chosen variable, $\hat{f}_n$, is larger than a specified threshold value $\hat{f}_c$. Hence, the two wavelet sets are defined by

$$\hat{\mathbf{f}}_H(l_x, l_y, z) = \begin{cases} \hat{\mathbf{f}}(l_x, l_y, z), & |\hat{f}_n(l_x, l_y, z)| \ge \hat{f}_c \\ 0, & |\hat{f}_n(l_x, l_y, z)| < \hat{f}_c \end{cases}$$

$$\hat{\mathbf{f}}_L(l_x, l_y, z) = \begin{cases} 0, & |\hat{f}_n(l_x, l_y, z)| \ge \hat{f}_c \\ \hat{\mathbf{f}}(l_x, l_y, z), & |\hat{f}_n(l_x, l_y, z)| < \hat{f}_c \end{cases}$$

for given (l_x, l_y, z), and $\hat{\mathbf{f}}(l_x, l_y, z) = \hat{\mathbf{f}}_H(l_x, l_y, z) + \hat{\mathbf{f}}_L(l_x, l_y, z)$.

The organization of convective cloud systems is largely controlled by wind shear (Moncrieff 1981). Jet-like wind profiles, where shear reverses with height, are

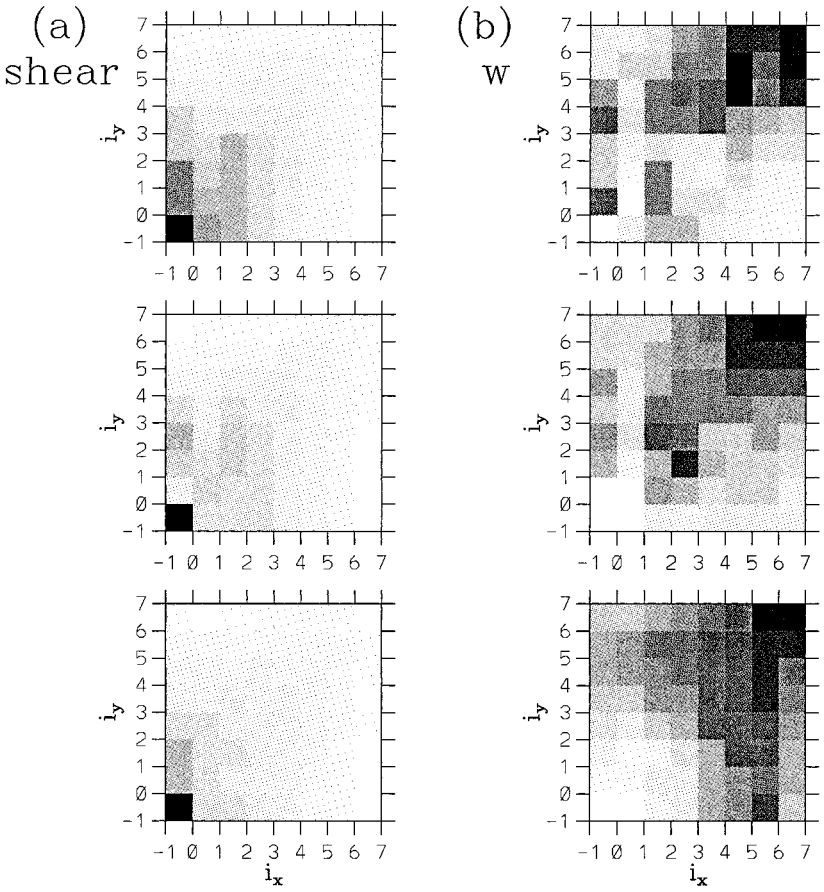

FIG. 2. The maximum pseudospectra for (a) the vertical wind shear $\partial|\hat{\mathbf{v}}_H|/\partial z$ and (b) the vertical velocity $\hat{w}$. The spectrum values are given by the gray tone defined in the logarithmic scale spanned from the minimum (lightest) to the maximum (darkest) of each spectrum. The coordinates are given by the wavenumber in x (horizontal) and y (vertical) directions, increasing by $k = 0, 1, 2, 4, \ldots, 64$ from the left (bottom) to the right (top: marked by the index i with the subscript for the coordinate directions, where $k = 2^i$ for $i \geq 0$ and $k = 0$ for $i = -1$). The cases shown are (top) the squall line, (middle) the nonsquall cloud cluster, and (bottom) scattered convection.

conductive to squall lines, a property demonstrated in idealized numerical simulations (Thorpe et al. 1982). In squall lines, shear organizes families of transient cumulonimbus (the convective scale) into a compact structure (the mesoscale convective system) that typically persists for much longer than the constituent cumulonimbus. This multicellular property and the attendant production of mesoscale circulation are clearly evident in the squall line simulations of Lafore and Moncrieff (1989) wherein the basic state was defined from measurements made during a field experiment. Mesoscale convective systems were analytically modeled by Moncrieff (1992) but a rigorous theory has not yet been developed for nonsquall clusters.

Convective systems are fundamentally affected by ambient wind shear, therefore we choose shear as a decomposition criterion. Specifically, we take the *wind-speed shear* $\partial|\hat{\mathbf{v}}_H|/\partial z$, as the criterion ($f_n$). The vertical derivative is computed by the centered finite differences with a linear extrapolation assumed over the vertical domain boundaries. We plot the vertically averaged maximum pseudospectrum for $\partial|\hat{\mathbf{v}}_H|/\partial z$ in Fig. 2a along with the same spectrum for the vertical velocity in Fig. 2b, reproduced from Figs. 12–14 of Part I. The mesoscale energy peaks identified for the squall line (top row) and the nonsquall cloud cluster (middle row) cases in Part I have counterparts in the shear spectrum. Hence, we anticipate that the wind speed shear is an appropriate criterion to distinguish the mesoscale from the convective scales: the high-shear component corresponds to the mesoscale mode and the low-shear component to the convective mode. The full wavelet spectra (not shown) indicate that both variables share the same spatial distribution at mesoscales.

Shear has a profound influence on mesoscale organization therefore we use it herein. We take the criterion variable as $\hat{f}_n = \partial|\hat{\mathbf{v}}_H|/\partial z$, and the threshold as $\hat{f}_c = \langle \hat{f}_n'^2 \rangle^{1/2}$, where $\langle\ \rangle$ and the prime designate the mean and

its deviation over the whole phase domain of (l_x, l_y, z)-space, respectively. This threshold is chosen such that the vertical mass flux is partitioned equally between the high-shear and the low-shear components in the squall line case (see section 3d). We obtain the physical-space structures for two decomposed modes by separately summing the two sets of classified wavelet coefficients by Eq. (4). The completeness and orthogonality of Meyer wavelets allow this decomposition procedure. An identical method was applied by Yamada and Ohkitani (1990) to a boundary-layer vertical velocity time series to distinguish a gusty period from a quiescent period but no attempt was made to correlate it with other variables.

c. Decomposed condensate fields

We apply the wavelet decomposition to the squall line, the nonsquall cloud cluster, and quasi-random scattered convection regimes. The results are shown in Figs. 3, 4, and 5, respectively, as snapshots of condensed water and ice fields. While our decomposition procedure applies to all dependent variables, the condensate field is particularly illustrative. In each figure, the top plate (a) represents the numerically simulated field (detailed in GWMH). The other two plates are the wavelet decomposition: (b) is the low-shear component and (c) the high-shear component. The three-dimensional domain is rotated to give the best perspective for each case. Orientation directions are indicated by *N* (north), *S* (south), *E* (east), and *W* (west).

Figure 3a is the numerical realization of the squall line, which occurred in an environment characterized by strong lower-tropospheric shear associated with the African easterly jet. The low-shear component of the wavelet decomposition (Fig. 3b) selects an ensemble of cumulonimbus, while the high-shear component of the decomposition successfully identifies the widespread stratiform and mesoscale ascent regions (Fig. 3c). In other words, the wavelet analysis and shear criterion have *objectively identified a scale dependence not assumed a priori.*

Figure 4a illustrates the simulated nonsquall cloud cluster, which occurs in moderate wind shear and features a less coherent spatial structure than the squall line. The wavelet decomposition nevertheless separates the total field into the two components. Note that the high-shear component (Fig. 4c) is of smaller scale than the corresponding component in the squall line case. The convection is also more intermittent as shown in the decomposed field (Fig. 4b).

Figure 5a represents scattered convection that typically occurs in weak shear conditions. Comparison of the wavelet fields shows that the simulated systems decompose into the convective-scale component (Fig. 5b) but the mesoscale component (Fig. 5c) is absent.

Our wavelet decomposition is based on the hypothesis that a shear criterion is sufficient to identify the con-

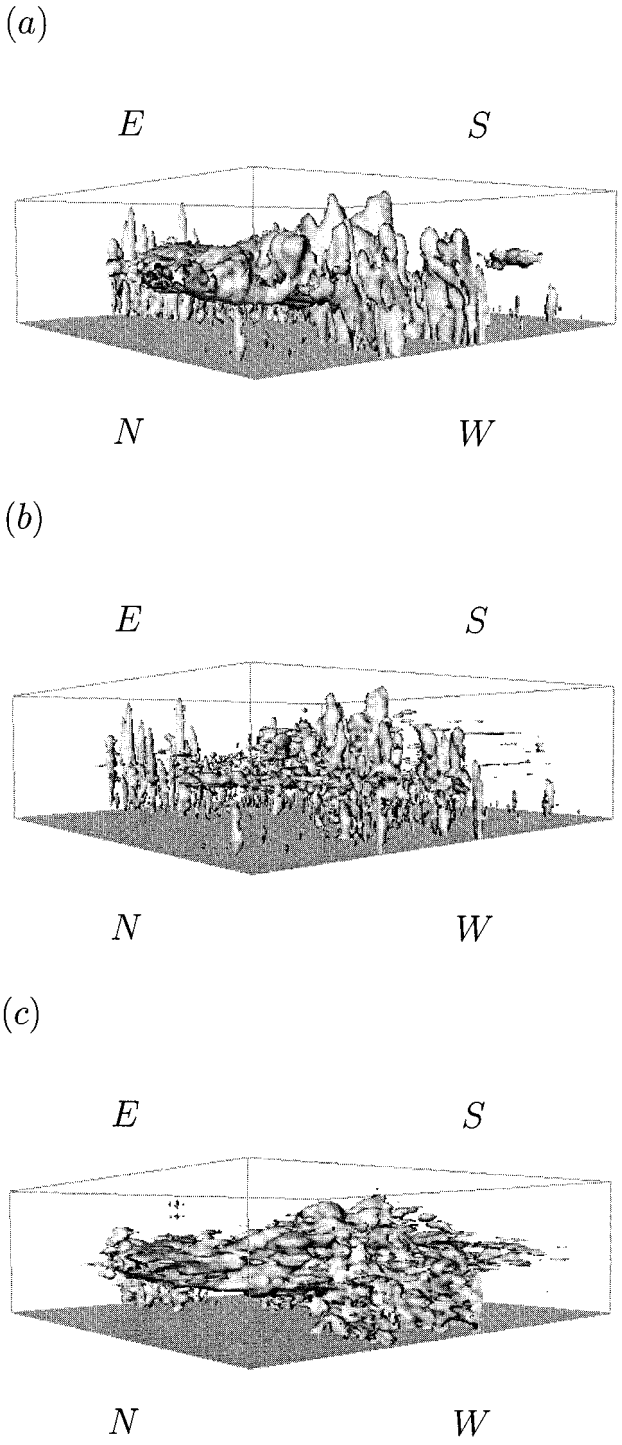

FIG. 3. A three-dimensional view of the simulated squall line. (a) The total condensed water and ice field and (b) its wavelet decomposition into the low-shear, and (c) the high-shear components. The direction of the three-dimensional frame is indicated by *N* (north), *S* (south), *E* (east), *W* (west). The domain is 400 km × 400 km × 16 km.

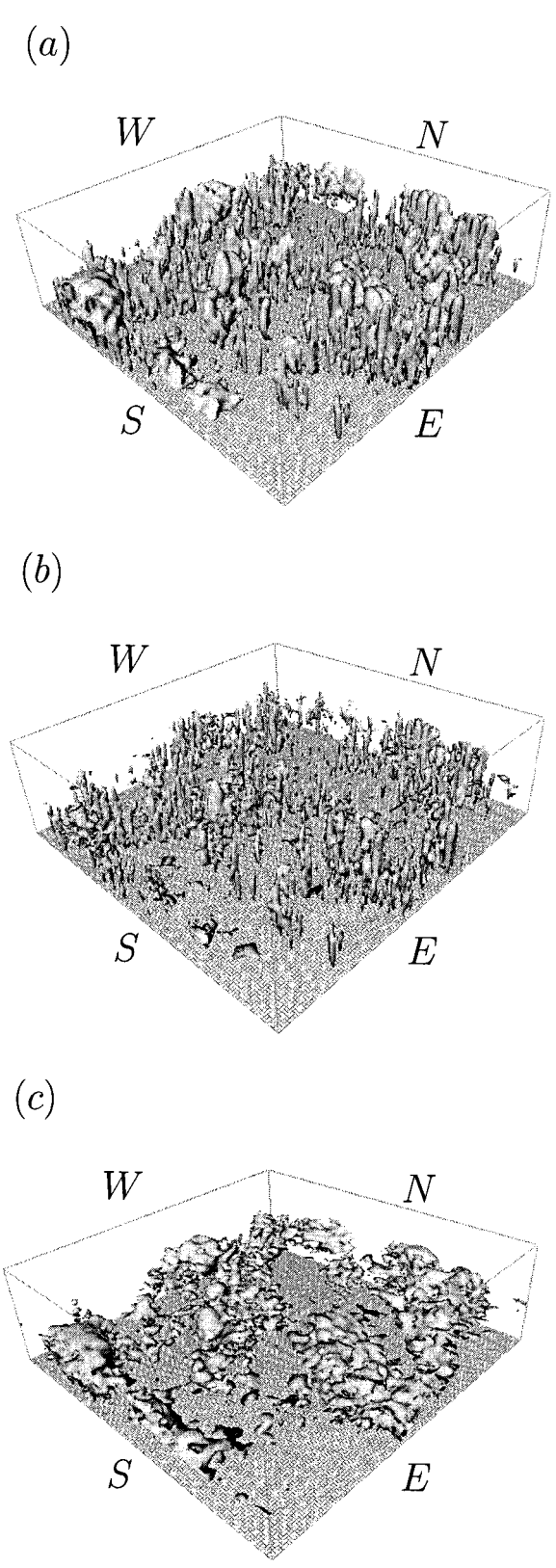

FIG. 4. The same as Fig. 3 but for the nonsquall cloud cluster regime. The three-dimensional frame is rotated to give the best perspective.

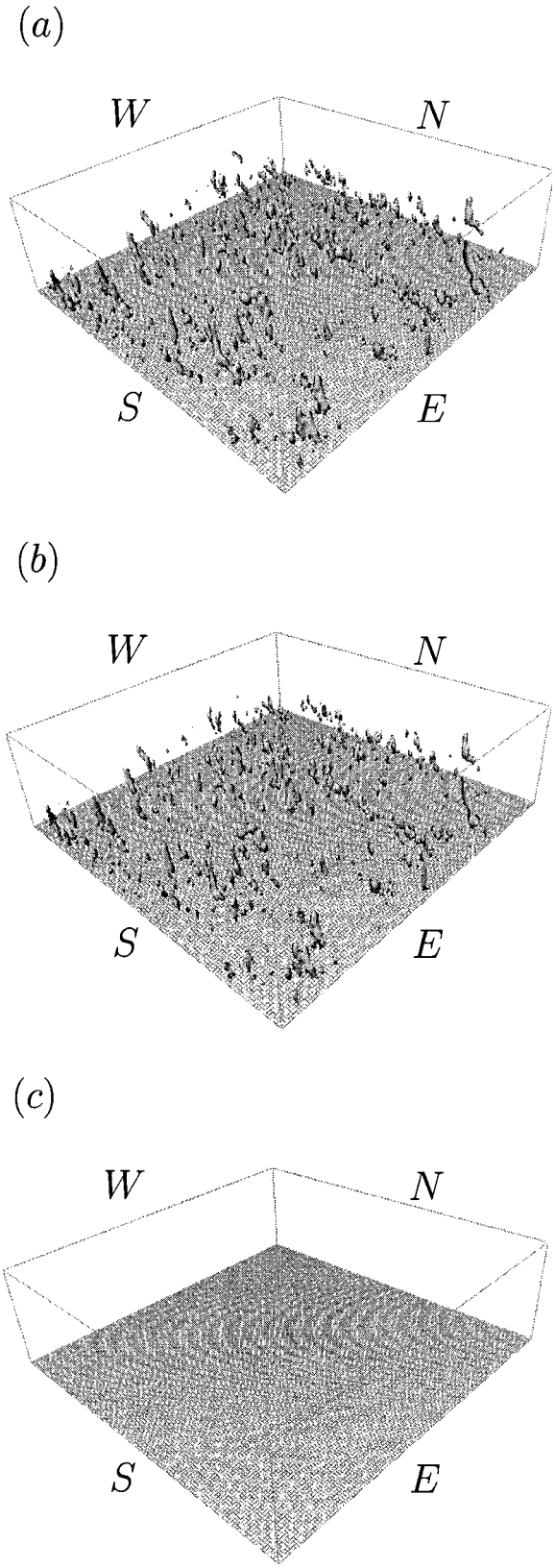

FIG. 5. The same as Fig. 3 but for the scattered convection regime.

vective from the mesoscale components. While the large-scale wind profile controls the convective organization (see introduction), there is no guarantee it would be useful in an objective decomposition of the simulated fields without evoking an explicit scale-dependent criterion.

The analysis of the squall line case (Fig. 3) reproduced features identified in a subjective analysis of such systems and clearly separates the convective-scale and the mesoscale components. The less organized nonsquall cloud clusters are decomposed in Fig. 4, where the mesoscale component has a smaller spatial size, consistent with the dynamics of these systems. The stochastic scattered convection in Fig. 5 is the null test passed by the wavelet procedure; that is, mesoscale organization was not expected and none occurs.

d. Mass fluxes

Our decomposition method can be used to obtain quantities relevant to convective parameterization in objective statistical terms (cf. Donner 1993; Alexander and Cotton 1998). As an example, we computed upward and downward mass fluxes for the total field and for the decomposed fields. We define the upward and downward mass fluxes by

$$M_\uparrow = \int \rho w_\uparrow \mathcal{H}(t_c - t_0)\, dx\, dy \Big/ \int dx\, dy,$$

$$M_\downarrow = \int \rho w_\downarrow \mathcal{H}(t_c - t_0)\, dx\, dy \Big/ \int dx\, dy,$$

respectively, where $w_\uparrow = w\mathcal{H}(w)$, $w_\downarrow = w\mathcal{H}(-w)$, and $\mathcal{H}(x)$ is the Heaviside step function. The horizontal integral is performed over the whole domain. The corresponding decomposed components, say, $w_{\uparrow H}$, $w_{\downarrow H}$, $w_{\uparrow L}$, and $w_{\downarrow L}$, are used for the vertical velocities in order to compute the mass fluxes $M_{\uparrow H}$, $M_{\downarrow H}$, $M_{\uparrow L}$, and $M_{\downarrow L}$ for decomposed fields, whereas the density ρ and the total water condensate t_c are kept as the total field. The threshold total condensate is $t_0 = 0.1$ g kg^{-1}. In this convention, the linear sum of the decomposed total mass fluxes $M \equiv M_\uparrow + M_\downarrow$ recovers the total mass flux for the total field $M = M_H + M_L$. The separate sum of the upward and downward components does not exactly recover the total (i.e., $M_\uparrow \neq M_{\uparrow H} + M_{\uparrow L}$ and $M_\downarrow \neq M_{\downarrow H} + M_{\downarrow L}$), because the decomposed upward motion area does not necessarily correspond to an upward motion in the total field. For example, a grid point with mesoscale downdraft may have a positive upward velocity in the total due to a strong embedded convective updraft.[2]

The results are shown in Fig. 6 for the squall line, the nonsquall cloud cluster, and the scattered convection cases. The solid curves represent the mass fluxes for the total field, the long-dash curves the high-shear component (mesoscale), and the short-dash curves the low-shear component (convective scale). The upward and downward fluxes are represented by positive and negative values, respectively.

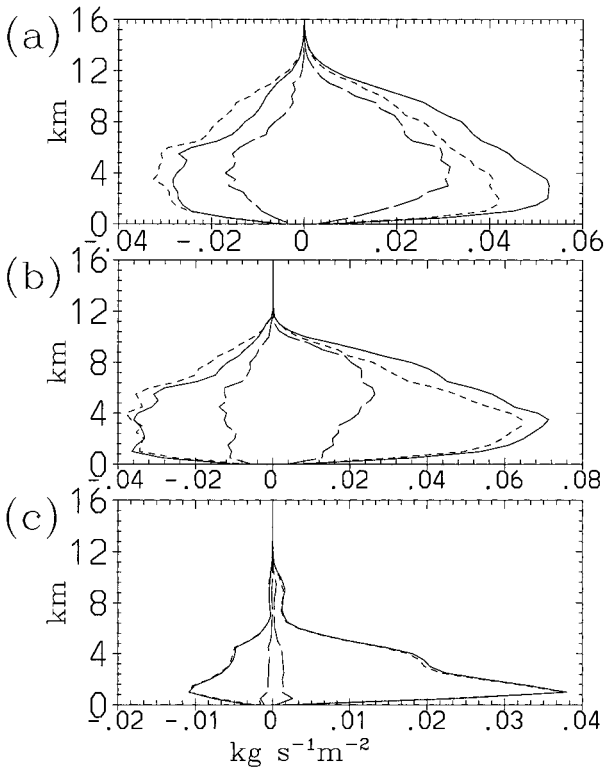

FIG. 6. The vertical profile of the upward and downward mass fluxes for the total field (solid), the high-shear component (long-dash), and the low-shear component (short-dash): (a) the squall line, (b) the nonsquall cloud cluster, and (c) the scattered convection cases. The upward and downward fluxes are represented by positive and negative values, respectively, in the unit of kg s^{-1} m^{-2}.

With a threshold of the standard deviation of the wind shear, the high-shear and the low-shear components contribute about equally to the mass flux in the squall line case. The high-shear component provides a larger contribution at the lower levels, presumably due to mesoscale downdrafts. The vertical profile of the low-shear mass flux is distributed more homogeneously. The contribution of the high-shear component decreases and its vertical structure is more homogeneous for the nonsquall cloud cluster case. In the scattered convection case, the mass flux is explained mostly by the low-shear (convective) component, and the high-shear component constitutes only a weak up-and-down couplet.

The above decomposed mass-flux analysis can be compared with a more traditional approach based on the columnwise classification in physical space. The precipitation rate is often used as a criterion variable for such columnwise classification (cf. Houze 1977; Tao and Simpson 1989). Note that Churchill and Houze (1984),

[2] Note that $M_H = M_{\uparrow H} + M_{\downarrow H}$ and $M_L = M_{\uparrow L} + M_{\downarrow L}$.

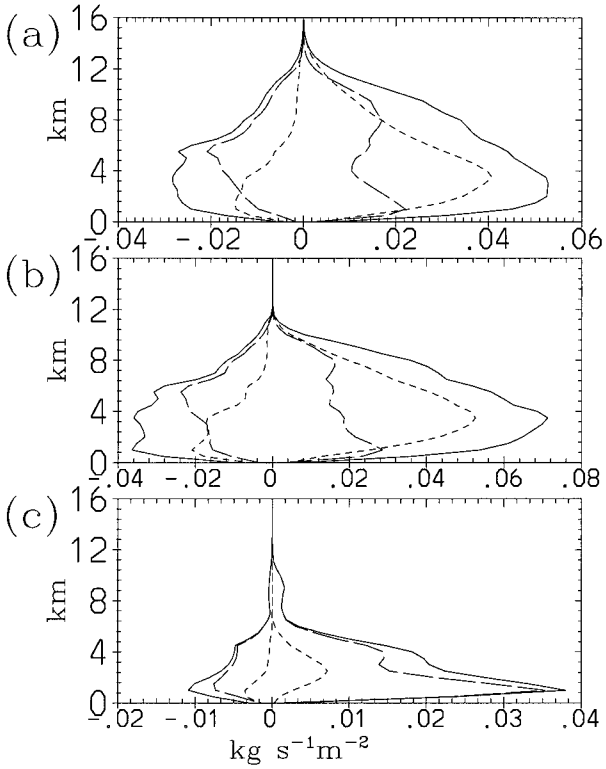

FIG. 7. The same as Fig. 6 but based on the columnwise decomposition in physical space.

Tao and Simpson (1989), Steiner et al. (1995), and Xu (1995) take some account of spatial structures. For a simple comparison, we prefer a method strictly based on individual columns as in Houze (1977) that has the same level of complexity as our wavelet decomposition. We therefore classify columns with a precipitation rate higher than 4 mm h^{-1} as the convective component and all the other columns as the mesoscale component. The result is shown in Fig. 7 in the same format as Fig. 6.

A familiar decomposition of the mass flux into the convective and the mesoscales (cf. Fig. 18 of Tao and Simpson 1989) is qualitatively reproduced in the squall line (not shown). In some respects, this physical space decomposition has a more attractive feature in that the sum of the decomposed upward and downward mass fluxes recover the total upward and downward values, that is, $M_{\uparrow} = M_{\uparrow H} + M_{\uparrow L}$ and $M_{\downarrow} = M_{\downarrow H} + M_{\downarrow L}$, separately. However, the contribution of the convective updrafts and downdrafts is substantially smaller compared to the wavelet-space decomposition, because overlapping convective and mesoscale areas are not taken into account. The unfavorable feature with the physical-space method is that the mass flux is mostly classified as a mesoscale component for the scattered convection case, wherein the mesoscale component should be absent. This occurs because the physical-space rainfall rate criterion does not by itself reflect dynamical aspects. Also lower-level mesoscale downdrafts are not well captured in the squall line case by this method. Rather, convective downdrafts are shallower and confined to the lower level (cf. Fig. 4 of Xu 1995).

The methods of Tao and Simpson (1989) and Xu (1995) were also examined. However, the improvement of the results (not shown) in terms of reduction of the mesoscale component in the scattered convection case was hardly worthwhile in view of the increased complexity. Rather, this demonstrates the strength of our method: by moving to wavelet space, a simple threshold condition can effectively decompose the fields.

4. Conclusions

Process studies have provided insight into the structure of mesoscale convective systems, but statistical aspects have received scant attention. Only recently have cloud-resolving models successfully simulated cloud systems and transitions among regimes as the large-scale conditions evolve in response to observed large-scale forcing. This success stems from two points: (i) the organizing effect of ambient wind shear on mesoscale dynamics and (ii) the parameterized microphysical processes being coupled by resolved cloud-scale dynamics. Simulations of highly organized squall lines, intermittent nonsquall cloud clusters, and quasi-random scattered convection, which mimic the real systems, were decomposed into convective-scale and mesoscale components. Wind shear was used as a decomposition criterion. The successful demonstration of the wavelet methodology with representative cases encourages an analysis of the week-long synthetic dataset using an automated procedure.

A three-dimensional simulation was performed by Wu et al. (1997) of a 2-week period during the Tropical Ocean Global Atmosphere Coupled Ocean–Atmosphere Research Experiment conducted over the western Pacific warm pool November 1992–February 1993. Convection was more transient, more intermittent, and featured organization on larger scales than in GATE, perhaps because the forcing was less compact. The wavelet analysis should be useful for quantifying differences in cloud system properties and the role of wind shear in these two major field experiments.

High-resolution global models are beginning to explicitly treat the largest tropical mesoscale convective systems (superclusters) in a surrogate way (Moncrieff and Klinker 1997), which is at odds with the assumptions of scale separation upon which convective parameterization is based. Furthermore, deep upper-tropospheric mesoscale outflow from these systems generate cirrus, which affects radiative transfer in key ways. Wavelet analysis of datasets from ground-based wind profilers in the tropical western Pacific (Gage et al. 1994) and space-based observations from the Tropical Rainfall Measuring Mission (TRMM)[3] should help quantify these issues.

[3] Information is available on the TRMM web site http://trmm.gsfc.nasa.gov.

Acknowledgments. J.I.Y. is supported by the Australian Government Cooperative Research Centre Program.

REFERENCES

Alexander, G. D., and W. R. Cotton, 1998: The use of cloud-resolving simulations of mesoscale convective systems to build a mesoscale parameterization scheme. *J. Atmos. Sci.,* **55,** 2137–2161.

Churchill, D. D., and R. A. Houze Jr., 1984: Development and structure of winter monsoon cloud clusters on 10 December 1978. *J. Atmos. Sci.,* **41,** 933–960.

Cotton, W. R., and R. A. Anthes, 1989: *Storm and Cloud Dynamics.* International Geophysics Series, Vol. 44, Academic Press, 883 pp.

Donner, L. J., 1993: A cumulus parameterization including mass fluxes, vertical momentum dynamics, and mesoscale effects. *J. Atmos. Sci.,* **50,** 889–906.

Farge, M., 1992: Wavelet transforms and their applications to turbulence. *Ann. Rev. Fluid Mech.,* **24,** 395–457.

Gage, K. S., C. R. Williams, and W. L. Ecklund, 1994: UHF wind profilers: A new tool for diagnosing tropical convective cloud systems. *Bull. Amer. Meteor. Soc.,* **75,** 2289–2294.

Grabowski, W. W., X. Wu, and M. W. Moncrieff, and W. D. Hall, 1998: Cloud-resolving modeling of tropical cloud systems during Phase III of GATE. Part II: Effects of resolution and the third spatial dimension. *J. Atmos. Sci.,* **55,** 3264–3282.

Houze, R. A., Jr., 1977: Structure and dynamics of a tropical squall-line system. *Mon. Wea. Rev.,* **105,** 1540–1567.

——, 1997: Stratiform precipitation in regions of convection: A meteorological paradox? *Bull. Amer. Meteor. Soc.,* **78,** 2179–2196.

——, S. A. Rutledge, M. L. Biggerstaff, and B. F. Smull, 1989: Interpretation of Doppler weather displays of midlatitude mesoscale convective systems. *Bull. Amer. Meteor. Soc.,* **70,** 608–619.

Lafore, J.-P., and M. W. Moncrieff, 1989: A numerical investigation of the organization and interaction of the convective and stratiform regions of tropical squall lines. *J. Atmos. Sci.,* **46,** 521–544.

McWilliams, J. C., and J. B. Weiss, 1994: Anisotropic geophysical vortices. *Chaos,* **4,** 305–311.

Meyer, Y., 1992: *Wavelets and Operators.* Cambridge University Press, 223 pp.

Moncrieff, M. W., 1981: A theory of organized steady convection and its transport properties. *Quart. J. Roy. Meteor. Soc.,* **107,** 29–50.

——, 1992: Organized convective systems: Archetypal dynamical models, mass and momentum flux theory, and parametrization. *Quart. J. Roy. Meteor. Soc.,* **118,** 819–850.

——, 1995: Mesoscale convection from a large-scale perspective. *Atmos. Res.,* **35,** 87–112.

——, and E. Klinker, 1997: Organized convective systems in the tropical western Pacific as a process in general circulation models: A TOGA COARE case study. *Quart. J. Roy. Meteor. Soc.,* **123,** 805–827.

Steiner, M. S., R. A. Houze Jr., and S. E. Yuter, 1995: Climatological characterization of three-dimensional storm structure from operational radar and rain gauge data. *J. Appl. Meteor.,* **34,** 1978–2007.

Tao, W.-K., and J. Simpson, 1989: Modeling study of a tropical squall-type convective line. *J. Atmos. Sci.,* **46,** 177–202.

Thorpe, A. J., M. J. Miller, and M. W. Moncrieff, 1982: Two-dimensional convection in non-constant shear: A model of mid-latitude squall lines. *Quart. J. Roy. Meteor. Soc.,* **108,** 739–762.

Wu, X., and M. W. Moncrieff, 1996: Recent progress on cloud-resolving modeling of TOGA COARE and GATE cloud systems. *Proc. New Insights and Approaches to Convective Parameterization Workshop,* Reading, United Kingdom, European Centre for Medium-Range Weather Forecasts, 128–156.

——, W. W. Grabowski, and M. W. Moncrieff, 1997: Three-dimensional cloud-resolving modeling of tropical convection on a time scale of one week. Preprints, *22d Conf. on Hurricanes and Tropical Meteorology,* Fort Collins, CO, Amer. Meteor. Soc., 65–66.

Xu, K.-M., 1995: Partitioning mass, heat, and moisture budgets of explicitly simulated cumulus ensembles into convective and stratiform components. *J. Atmos. Sci.,* **52,** 551–573.

Yamada, M., and K. Ohkitani, 1990: Orthonormal wavelet expansion and its application to turbulence. *Prog. Theor. Phys.,* **83,** 819–823.

Yano, J.-I., M. W. Moncrieff, X. Wu, and M. Yamada, 2001: Wavelet analysis of simulated tropical convective cloud systems. Part I: Basic analysis. *J. Atmos. Sci.,* **58,** 850–867.